

Murine bilateral retinoblastoma exhibiting rapid-onset, metastatic progression and *N-myc* gene amplification

David MacPherson^{1,*}, Karina Conkrite¹,
Mandy Tam², Shizuo Mukai³, David Mu⁴
and Tyler Jacks^{2,5}

¹Department of Embryology, Carnegie Institution, Baltimore, MD, USA, ²Center for Cancer Research, Massachusetts Institute of Technology, Cambridge, MA, USA, ³Massachusetts Eye and Ear Infirmary and Harvard Medical School, Boston, MA, USA, ⁴Human Cancer Genome Center, Cold Spring Harbor Laboratory, Woodbury, NY, USA and ⁵Howard Hughes Medical Institute, Chevy Chase, MD, USA

Human retinoblastoma is a pediatric cancer initiated by *RB* gene mutations in the developing retina. We have examined the origins and progression of retinoblastoma in mouse models of the disease. Retina-specific inactivation of *Rb* on a *p130*^{-/-} genetic background led to bilateral retinoblastoma with rapid kinetics, whereas on a *p107*^{-/-} background *Rb* mutation caused predominantly unilateral tumors that arose with delayed kinetics and incomplete penetrance. In both models, retinoblastomas arose from cells at the extreme periphery of the murine retina. Furthermore, late retinoblastomas progressed to invade the brain and metastasized to the cervical lymph nodes. Metastatic tumors lacking *Rb* and *p130* exhibited chromosomal changes revealed by representational oligonucleotide microarray analysis including high-level amplification of the *N-myc* oncogene. *N-myc* was found amplified in three of 16 metastatic retinoblastomas lacking *Rb* and *p130* as well as in retinoblastomas lacking *Rb* and *p107*. *N-myc* amplification ranged from 6- to 400-fold and correlated with high *N-myc*-expression levels. These murine models closely resemble human retinoblastoma in their progression and secondary genetic changes, making them ideal tools for further dissection of steps to tumorigenesis and for testing novel therapies.

The EMBO Journal (2007) 26, 784–794. doi:10.1038/sj.emboj.7601515; Published online 18 January 2007

Subject Categories: cell cycle; molecular biology of disease

Keywords: *N-myc*; *p107*; *p130*; retinoblastoma; ROMA

Introduction

In humans, inherited and somatic mutations in the *RB* tumor suppressor gene lead to the development of retinoblastoma, a childhood malignant tumor of the eye. In contrast, germline heterozygosity for *Rb* gene mutations in mice causes predis-

position to pituitary and thyroid tumors, but these animals do not develop retinoblastoma (Clarke *et al*, 1992; Jacks *et al*, 1992). Homozygous *Rb* mutation results in mid-gestational embryonic lethality, which has been attributed to defects in placental and hematopoietic development (Clarke *et al*, 1992; Jacks *et al*, 1992; Lee *et al*, 1992; Wu *et al*, 2003). We and others have specifically deleted *Rb* in the developing mouse retina using Cre-lox technology (Chen *et al*, 2004; MacPherson *et al*, 2004; Zhang *et al*, 2004a). Use of *Pax6* α -*Cre* transgenic mice to delete *Rb* in early retinal progenitors led to defects in proliferation, increased levels of cell death and associated inhibition of differentiation in a cell-type-specific fashion. The majority of bipolar, ganglion and many rod photoreceptor cells were selectively lost in the developing *Rb*-deficient retina, whereas other cell types survived (Chen *et al*, 2004; MacPherson *et al*, 2004). Although *Rb* deletion leads to proliferation defects in the retina, retinoblastomas did not develop.

Compensation or functional overlap affecting the activity or levels of the pocket protein family members, p107 and p130, minimizes the effects of *Rb* loss, preventing tumorigenesis. This was first shown in a chimeric setting, where retinoblastomas did not emerge in chimeras with retinal contribution of *Rb*^{-/-} cells (Maandag *et al*, 1994; Williams *et al*, 1994), but were present in chimeras composed of cells mutant for both *Rb* and *p107* (Robanus-Maandag *et al*, 1998). Breedable models of retinoblastoma involving conditional *Rb* mutation on a *p107*^{-/-} genetic background (with or without additional *p53* inactivation) have now been generated (Chen *et al*, 2004; Zhang *et al*, 2004b). We recently used transgenic expression of Cre from the *nestin* promoter to show that inactivation of *Rb* in neural progenitors of *p130*^{-/-} animals also results in retinoblastoma development (MacPherson *et al*, 2004).

The apparent functional compensation among the *Rb* gene family may explain the fact that in many human tumors the *RB* pathway is disrupted not by *RB* mutation, but by mutations that act upstream (reviewed in (Sherr, 1996)). Examples include *p16*^{INK4a} loss in glioma, melanoma and pancreatic carcinoma, *CDK4* amplification in melanoma, *cyclin D1* amplification in breast and esophageal cancer or translocations in B-lineage tumors. Thus, examining tumor formation in a context of mutation in multiple *Rb* family members in the mouse may help us understand the overlapping and unique roles of these proteins in tumor suppression.

The availability of well-defined mouse models of retinoblastoma is expected to help answer longstanding questions concerning the genetic changes that contribute to retinoblastoma progression as well as the nature of the cell of origin of this tumor type. For example, Knudson's two-hit hypothesis proposed that mutations in both alleles of the *RB* gene represent the rate-limiting steps in retinoblastoma development (Knudson, 1971). However, comparative genomic

*Corresponding author. Department of Embryology, Carnegie Institution, 3520 San Martin Drive, Baltimore, MD 21218, USA. Tel.: +1 410 246 3084; Fax: +1 410 243 6311; E-mail: macpherson@ciwemb.edu

Received: 11 August 2006; accepted: 28 November 2006; published online: 18 January 2007

hybridization (CGH) analysis has revealed chromosomal gains at 6p, 1q and 2p as well as losses at 16q in a significant percentage of human retinoblastomas (Mairal *et al*, 2000; Chen *et al*, 2001; Lillington *et al*, 2003; Zielinski *et al*, 2005). These data suggest that other changes also occur during tumor progression. In particular, selection for *N-myc* amplification has been implicated in the 2p gain, which often involves high-level gene amplifications (Lee *et al*, 1984).

Microarray-based CGH platforms in which tumor or normal DNA is hybridized to bacterial artificial chromosomes (BAC), cDNA or oligonucleotide arrays are improving the resolution with which copy number changes can be detected (reviewed in Pinkel and Albertson, 2005). Representational oligonucleotide microarray analysis (ROMA) is a comparatively new approach for detecting copy number variation that uses PCR-based genome representations hybridized to oligonucleotide arrays, reducing genome complexity and increasing signal-to-noise ratios (Lucito *et al*, 2003; Lakshmi *et al*, 2006). Application of ROMA to mouse models of retinoblastoma, where tumor progression can be examined in a more controlled and less variable manner than possible using human samples, may aid in the identification of secondary changes also relevant for tumor progression.

In this study, we use improved mouse models of retinoblastoma to examine tumor initiation and progression to metastatic disease. We also show that ROMA analysis can identify an important secondary oncogenic event that contributes to tumor development in these models, pinpointing a minimal region of gene amplification that includes a single known gene.

Results

Mutation of *Rb* coupled with the absence of either *p107* or *p130* in chimeric or in retina-specific knockout models causes retinoblastoma (Robanus-Maandag *et al*, 1998; Chen *et al*, 2004; Dannenberg *et al*, 2004; MacPherson *et al*, 2004; Zhang *et al*, 2004b). These results may suggest that retinoblastoma development results from an overall reduction in 'Rb family' tumor suppressor function, which can occur equivalently through loss of pRB plus either of the *Rb*-related proteins. However, in some experiments involving compound mutation with *Rb*, distinct effects of *p107* and *p130* mutations have been shown (Dannenberg *et al*, 2004; Haigis *et al*, 2006). Therefore, we directly compared the effects of *p107* versus *p130* mutation when combined with retinal-specific deletion of a conditional allele of *Rb* (MacPherson *et al*, 2003; Sage *et al*, 2003). For these studies, we used a transgenic strain in which *Cre* expression is controlled by the α -enhancer of the *Pax6* promoter. In *Pax6* α -enhancer *Cre* transgenic mice, *Cre* expression occurs by embryonic day (E)10.5 in mid- to far-peripheral neural retina as well as in some peripheral eye structures (Supplementary Figure 1; Marquardt *et al*, 2001). Here, we refer to animals with retinal-specific *Rb* mutation on *p107*^{-/-} or *p130*^{-/-} genetic backgrounds as *Rb/p107* double knockout (DKO) or *Rb/p130* DKO mice.

Kinetics of retinoblastoma development in *Rb/p107* versus *Rb/p130* DKO mice

We aged compound mutant mice and followed tumor development by visual examination of the mouse eye over time. Mice were examined for either the presence of tumor or blood

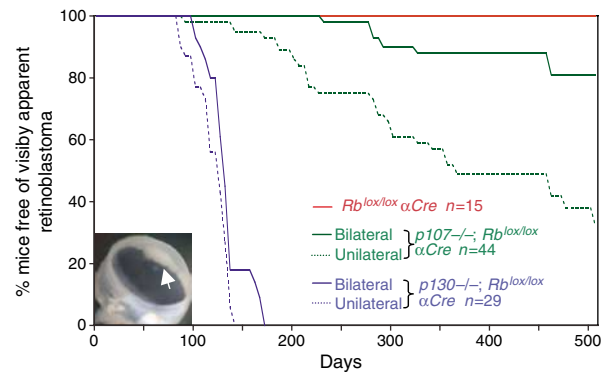


Figure 1 Different kinetics of retinoblastoma emergence in *Rb/p107* versus *Rb/p130* DKO mice. Kaplan-Meier curve showing time to first observation of externally visible retinoblastoma. Inset: retinoblastoma visible in the anterior chamber of an *Rb/p130* DKO mouse at 4 months of age.

in the anterior chamber, or distortion of the eye caused by the tumor. Upon initial observation of unilateral retinoblastoma, the cohort continued to be followed for the appearance of bilateral retinoblastoma unless tumor burden either in the eye region or due to metastasis necessitated killing of the animal. Figure 1 shows the time to first observation of retinoblastoma upon examination of the eye. *Rb/p130* DKO mice developed visible retinoblastoma with rapid and consistent kinetics, exhibiting an average time to visible bilateral retinoblastoma of 128 ± 18 days (mean \pm s.d). By contrast, mutation of *Rb* and *p107* led to tumors that developed with delayed and variable kinetics: 27/44 (61%) developed unilateral retinoblastoma, first visible at an average time of 280 ± 107 days. Bilateral tumors were rare in this *Rb/p107* DKO model (Figure 1). Overall, the tumor kinetic data indicate that the pattern of tumorigenesis in the *Rb/p107* DKO and *Rb/p130* DKO models differs significantly.

Rb/p130 DKO tumors emerge from the extreme periphery of retina

The rapid and consistent kinetics of tumor formation in *Rb/p130* DKO mice provided an opportunity to examine the origins of retinoblastoma development. We examined retinas histologically at postnatal day (PND)21, a time when retinal histogenesis is normally complete. Previous work by us and others has shown that the absence of *Rb* alone causes hypocellularity in the retina due to loss of specific cell types, but the three nuclear layers are still detected (Chen *et al*, 2004; MacPherson *et al*, 2004). In contrast, in the *Rb/p130* DKO mice, the three nuclear layers could not be distinguished, except in central retina, where *Cre* is not widely expressed (Figure 2A). The *Rb/p130* DKO retinas were very hypocellular and contained apoptotic bodies and many cells exhibiting large and/or irregular-shaped nuclei (Figure 2A, inset; data not shown). Strikingly, at the extreme periphery in 9/12 eyes examined, we observed early dysplastic lesions with histological similarities to retinoblastomas (Figure 2A, right). Such lesions contained Homer-Wright rosettes, which consist of a radial arrangement of cells surrounding a central tangle of neuronal processes and are found in a subset of human retinoblastomas (Yuge *et al*, 1995) as well as murine retinoblastomas (Robanus-Maandag *et al*, 1998; Dannenberg *et al*, 2004;

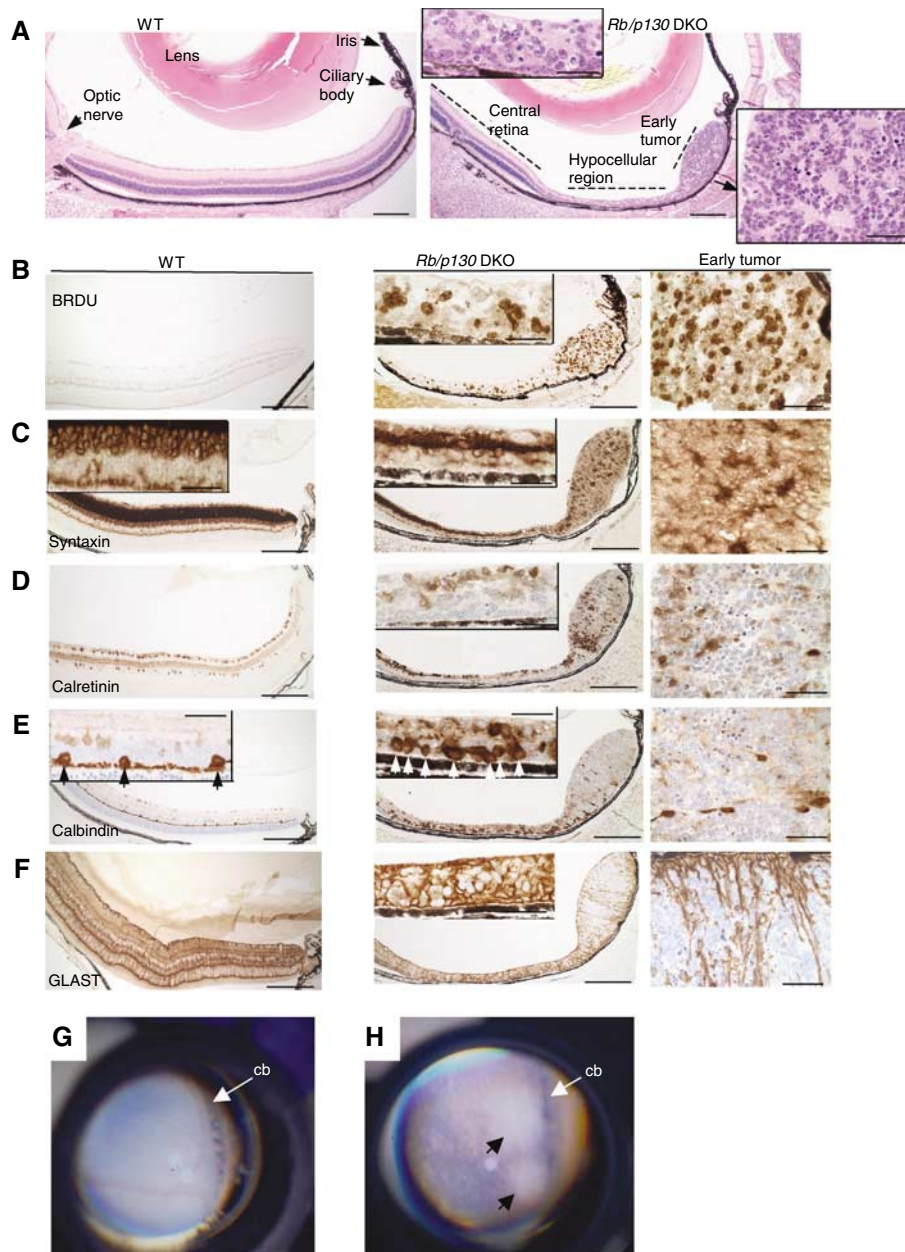


Figure 2 *Rb/p130* DKO tumors emerge from the extreme periphery of retina. Early retinoblastomas in *Rb/p130* DKOs. (A–F) Histology and immunostaining of PND21 retinas from wild-type (left panel) and *Rb/p130* DKO (middle, right panels) animals. The upper inset in the middle panel shows details of *Rb/p130* DKO retina adjacent to tumor. The panel in the right shows details from *Rb/p130* DKO early tumor. Scale bars in the left and middle low-power panels = 200 μ m, high-magnification insets and right panels, 40 μ m. (A) Hematoxylin and eosin (H + E) stain with normal eye structures labeled. Distinct regional phenotypes and early retinoblastoma in the *Rb/p130* DKO are noted. (B) BrdU labeling of proliferating cells. (C) Syntaxin immunostaining. Note the depletion of amacrine cells adjacent to tumor (inset, middle panel) and the positive staining of early retinoblastoma (right). (D) Calretinin immunostaining labeling an amacrine and ganglion subset. (E) Calbindin immunostaining. Arrows indicate calbindin-positive horizontal cells. (F) GLAST immunostaining labeling Müller glia. (G) Fundus photograph of a *p130*^{-/-} control mouse at 6 weeks of age. The ciliary body, peripheral to the neural retina, is indicated (white arrow). (H) Fundus photograph of *Rb/p130* DKO mouse at 6 weeks of age. Peripheral retina is shown and black arrows point to early retinoblastoma at the extreme periphery. Retinal pigment epithelial changes due to retinal degeneration are present. The ciliary body, adjacent to the neural retina, is indicated (white arrow).

MacPherson *et al*, 2004). The detection of early tumors specifically at the extreme periphery of the retina points to a possible niche for the cell of origin of retinoblastoma in this model. Importantly, these results do not simply reflect the expression of *Cre* in the extreme distal retina as *Pax6* α -*Cre* is expressed much more broadly (Supplementary Figure 1).

Loss of *Rb* leads to increased proliferation beyond the normal period of retinogenesis (Chen *et al*, 2004;

MacPherson *et al*, 2004). At PND12, we found extensive BrdU incorporation in *Rb*^{lox/lox} α -*Cre* retinas, and this phenotype was exacerbated in *Rb/p130* DKO retinas (Figure 3A and C). Inappropriate proliferation was accompanied by increased apoptosis, which was also found at higher levels in *Rb/p130* DKO over single *Rb* mutant retinas (Figure 3B and C). By PND21, proliferation could not be detected in *Rb* mutants (Chen *et al*, 2004; data not shown). In contrast,

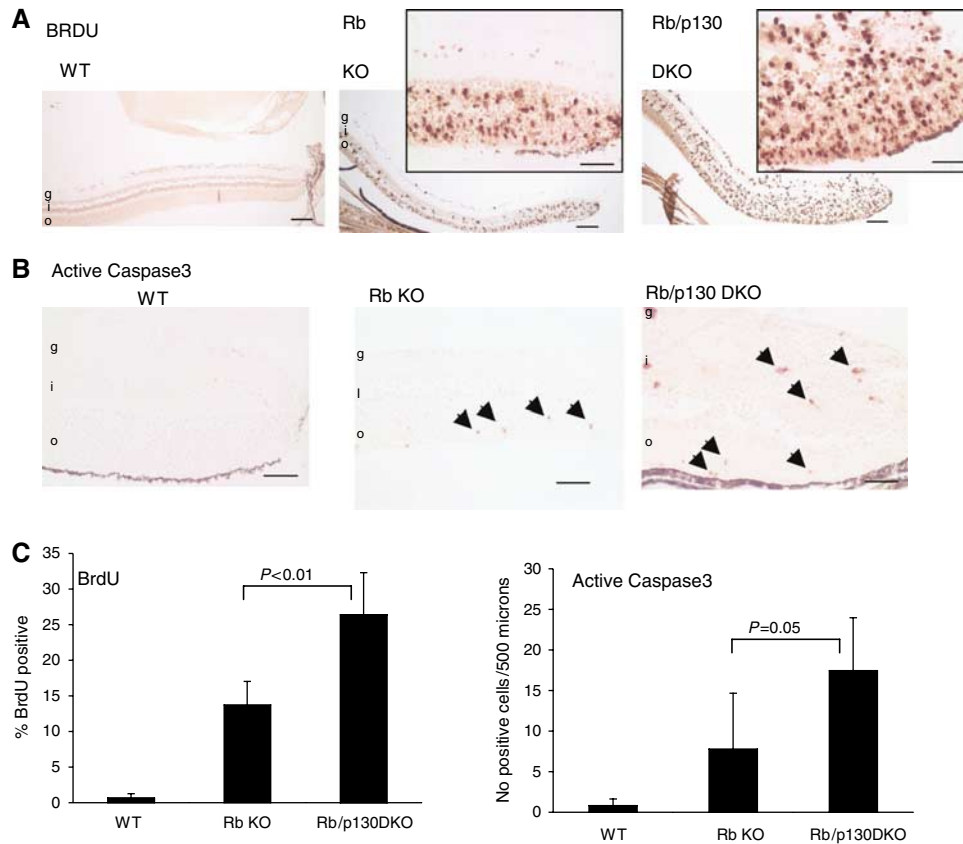


Figure 3 Proliferation and apoptosis in *Rb/p130* DKOs at PND12. (A) BrdU incorporation in retinas from wild-type, *Rb^{lox/lox} αCre* (*Rb* KO) and *Rb/p130* DKO animals. Ganglion (g), inner nuclear (i) and outer nuclear (o) layers are indicated. Scale bar = 200 μm (low magnification) and 40 μm (high magnification). (B) Caspase3 immunostaining in retinas from wild-type, *Rb^{lox/lox} αCre* and *Rb/p130* DKO animals. Scale bar = 40 μm. (C) Quantification of BrdU and Caspase3 staining. Quantification was performed on horizontal sections at the optic nerve level in a region from the peripheral tip of the retina extending 1000 μm toward central retina. WT *N* = 3; *Rb* KO *N* = 4, *Rb/p130* DKO *N* = 8. Error bars represent standard deviation. *P*-values (Student's *t*-test) are shown.

BrdU-positive cells were found in *Rb/p130* DKOs throughout the PND21 distal retina, and were particularly concentrated at the extreme periphery, where early tumors were detected (Figure 2B). BrdU-positive cells were also found away from the tumor regions (Figure 2B, middle panel inset) where the retina was hypocellular and were also found in PND21 *Rb/p130* DKO retinas that did not yet exhibit histological evidence of early retinoblastoma formation (data not shown). These data suggest that the combined loss of *Rb* and *p130* function in the retina causes broad defects in cell-cycle control, accompanied by cell death.

To characterize the early lesions further, we stained histological sections of *Rb/p130* DKO retinas at PND21 for cell-type markers. Consistent with previous descriptions of murine retinoblastomas lacking *Rb* and *p107* or *p130*, we found that early tumors expressed syntaxin, which stains amacrine cells and a subset of progenitor cells (Figure 2C) (Alexiades and Cepko, 1997). Away from the tumors, the amacrine layer was significantly reduced (Figure 2C, inset), suggesting that many amacrine cells do not survive in the absence of *Rb* and *p130* function. The early tumors also stained for calretinin, which labels a subset of amacrine and ganglion cells (see control retina; Figure 2D). Calretinin in the tumors was expressed in a more focal and heterogeneous fashion that was variable from animal to animal. In normal retina,

calbindin labels horizontal cells strongly (arrowheads) and a subset of amacrine cells weakly (Figure 2E). We found calbindin-positive cells in early tumors, including some intensely stained cells that were reminiscent of horizontal cells. Interestingly, adjacent to the early tumors, and in contrast to the overall hypocellularity in this area, *Rb/p130* DKO retinas exhibited a clear increase in horizontal cells (Figure 2E, middle panel inset). The glial glutamate/aspartate transporter (GLAST) labels Müller cells, which survived both *Rb* and *p130* mutation and were present in the early tumor (Figure 2F). At this stage, some of the cells present in the early tumors may be non-neoplastic cells derived from normal retina. A cone subset (stained for M-opsin; Zhu *et al*, 2003), rod bipolar cells (stained for PKCα) and Tuj1-positive retinal ganglion cells were either very rare or completely absent from the *Rb/p130* DKO retina and early tumors (data not shown).

Retinoblastoma progression in *Rb/p130* DKOs

Beyond PND21, cells in the periphery of *Rb/p130* DKO retinas continued to proliferate. Larger tumors were found at PND31 (four animals) and PND60 (three animals), and all mice at PND31 and PND60 had retinoblastomas in each eye. Upon ophthalmoscopic examination, early tumors could be visualized by 6–8 weeks, and these were adjacent to the ciliary

body at the extreme periphery of the neural retina (Figure 2H). By 4 months of age, retinoblastoma seeding the vitreous and anterior chamber of the eye was detected upon visual examination of the mouse (Figure 1). To investigate late-stage tumor progression, mice continued to be monitored beyond the initial observation of tumor until the mouse was moribund due to retinal tumor burden or retinoblastoma presence at sites outside of the eye. *Rb/p130* DKO mice were killed at an average age of 183 ± 39 days of age. By this advanced stage, retinoblastomas had grossly distended the eye, filled the anterior chamber and had often invaded local tissue outside of the eye (Figure 4A and B). Tumor cells could also be found infiltrating the optic nerve (Figure 4B). We found that 11/29 (38%) of these *Rb/p130* DKO mice exhibited enlarged cervical lymph nodes. Histological analysis revealed that these were retinoblastoma metastases (Figure 4C).

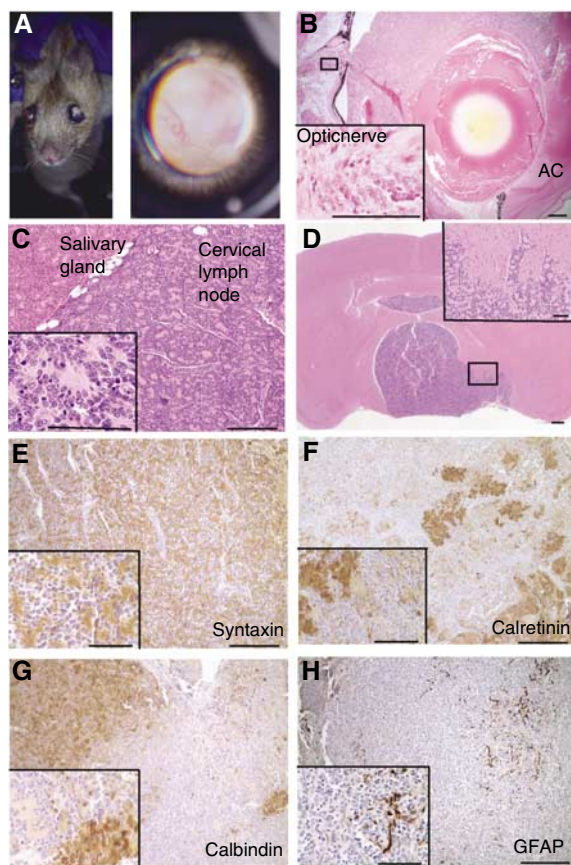


Figure 4 Tumor progression in murine *Rb/p130* DKO retinoblastoma. Histology and immunostaining of late retinoblastoma and metastases in *Rb/p130* DKO mice from 5 to 7 months of age. Scale bar = 200 μ m for low power and 60 μ m for high power (inset) images. (A) Bilateral retinoblastoma in a 5-month-old mouse (left). Fundus photograph of late-stage retinoblastoma that fills the vitreous at 5 months (right). (B) H + E stain of late retinoblastoma, with blood and tumor in the anterior chamber (AC) and invasion of the optic nerve (inset). (C) H + E stain of lymph node metastasis, adjacent to the salivary gland. Tumor rosettes are apparent on the high-magnification image (inset). (D) H + E stain of brain with retinoblastoma invading into brain parenchyma (inset). (E) Syntaxin immunohistochemistry of lymph node metastasis. (F) Calretinin immunohistochemistry of lymph node metastasis. (G) Calbindin immunohistochemistry of lymph node metastasis. (H) Glial fibrillary acidic protein (GFAP) immunohistochemistry of lymph node metastasis.

Although the kinetics of tumor development in the *Rb/p130* DKO model was consistent at early time points, the properties and size of the metastatic tumors varied significantly.

Human retinoblastoma is known to invade the brain via the optic nerve (Shields *et al*, 1994). Given the presence of retinoblastoma cells in the optic nerve in the mouse model, we examined 27 *Rb/p130* DKO animals for brain involvement. Seven animals were found to contain retinoblastoma lesions in the brain (26%, average age 199 ± 41 days) (Figure 4D). To determine whether tumors spread to other tissues as well, we performed full necropsies on eight *Rb/p130* DKO animals. Tumors were found only locally near the eye and surrounding tissues, in the brain and in cervical lymph nodes but not in other distant sites.

Tumor progression in *Rb/p107* DKOs

To further assess functional differences between *p130* and *p107* mutation, we also carefully examined tumor progression in the *Rb/p107* DKO animals. Although the *Rb/p107* DKOs exhibit slower tumor kinetics and incomplete retinoblastoma penetrance (Figure 1), the end-stage tumors were histologically similar to the *Rb/p130* DKO tumors (Figure 4B and C, and Supplementary Figure 2A). Because monitoring externally visible retinoblastomas may have led to an underestimation of the incidence of bilateral tumors in this model, we performed histological examination of the second eye in 11 *Rb/p107* DKO animals killed due to unilateral retinoblastoma tumor burden. Retinas from all 11 eyes exhibited disorganization and degeneration, and 3/11 retinas contained an early retinoblastoma. These early lesions had abundant mitotic figures, high levels of apoptosis and Homer–Wright rosettes (data not shown).

To determine whether the extreme peripheral localization of early tumors seen in the *Rb/p130* DKO model was also applicable to the *Rb/p107* DKO model, we examined *Rb/p107* DKOs at PND31 and PND60 by histological analysis. At PND60, obvious retinoblastomas were present in four of 14 eyes examined at the level of the optic nerve head, and, in each case, the tumor was present at the extreme periphery of the retina (Supplementary Figure 3A). In 6/24 eyes examined at PND31, dysplastic lesions containing Homer–Wright rosettes were seen in this location, suggestive of early retinoblastoma. Moreover, BrdU-labeling studies performed at PND31 demonstrated proliferation concentrated at the extreme retina periphery in *Rb/p107* DKOs that did not yet exhibit histological evidence of retinoblastoma (Supplementary Figure 3B and C). These data point to peripheral, late-proliferating cells as candidates for the cell of origin in the *Rb/p107* DKO model as well.

Consistent with overall tumor progression in this model, metastatic spread was also delayed in the *Rb/p107* DKO model. In 4/14 *Rb/p107* DKO mice examined histologically, retinoblastoma was observed in the CNS (average age of 296 ± 68 days). We also observed metastasis to the cervical lymph nodes in *Rb/p107* DKO mice.

Late-stage retinoblastomas are heterogeneous

To further characterize the cell-type composition of metastatic tumors, we studied the expression of other retinal cell-type markers in metastases from *Rb/p107* DKO and *Rb/p130* DKO mice. We focused on lymph node metastases, which are less likely than primary tumors to have infiltration of

non-tumor cells from normal retina. *Rb/p107* DKO and *Rb/p130* DKO metastases stained positively for syntaxin (Figure 4E and Supplementary Figure 2B), whereas calretinin stained *Rb/p130* and *Rb/p107* DKO metastatic tumors in a patchy pattern, variable from animal to animal (Figure 4F and Supplementary Figure 2B). Calbindin was found to strongly label tumor cells in late lesions in the *Rb/p130* DKOs, suggestive of a horizontal cell component to the tumors. This staining was also variable, ranging from only scattered positive cells in some tumors to others in which the majority of cells stained strongly (Figure 4G). In *Rb/p107* DKOs, calbindin staining was typically found in a more scattered pattern (Supplementary Figure 2B) and many tumors were completely negative, indicative of some difference in the composition of *Rb/p107* versus *Rb/p130* DKO tumors. Some *Rb/p130* and *Rb/p107* DKO tumors exhibited glial fibrillary acidic protein (GFAP) and GLAST positivity (Figure 4H and Supplementary Figure 2B; data not shown). GFAP staining in retinoblastomas has been observed in murine and human retinoblastoma, but reactive gliosis from nearby Müller cells has often been implicated. GFAP and GLAST staining in the metastatic tumors in cervical lymph nodes is significant as it suggests that the Müller glial cells may indeed derive from tumor cells. This population was, however, a minor component and not present in all tumors.

Overall, these data show that, although they progress at different rates, the retinoblastomas arising in *Rb/p107* DKO and *Rb/p130* DKO animals share many characteristics, including site of origin, overall histological appearance and routes to invasion and metastasis.

ROMA analyses of murine retinoblastomas

Although combined mutation in *Rb* and either *p107* or *p130* produced retinoblastomas at high frequency, the tumors were focal and, presumably, clonal. Thus, it is likely that additional genetic events contribute to tumor progression. To begin to catalog these changes, we utilized ROMA, a form of array CGH that uses PCR-generated genome representation to measure genomic DNA copy number alterations (Lucito *et al*, 2003). To maximize the chances of finding clonal genomic changes, we focused on metastatic tumors isolated from *Rb/p130* DKO mice; six tumors were tested initially. As summarized in Table I, recurrent changes were identified in this tumor collection. For example, whole chromosome gains were frequently observed for chromosomes 1 and 12. These chromosomes may harbor one or multiple genes that contribute to tumorigenesis when expression is increased. More informatively, we also found focal regions of high-level amplification in a subset of tumors (Table I).

N-myc amplification in a subset of murine retinoblastomas

In our initial sampling of six tumors, we observed some focal amplifications, including two amplicons in tumor 9806 at 12qA1.1 and 12qF2 (Table I, and Figure 5A). Interestingly, the *N-myc* oncogene resides on 12qA1.1, and this gene has been reported to be amplified in approximately 10% of human retinoblastomas (Lee *et al*, 1984; Squire *et al*, 1986; Mairal *et al*, 2000; Lillington *et al*, 2002). To confirm the results from ROMA as well as to examine additional tumors, we performed Southern blot analyses of tumor DNA using *N-myc* as a probe. As shown in Figure 5, among metastatic tumors in

Table I ROMA analysis of chromosomal changes in metastatic *Rb/p130*DKO retinoblastomas

Tumor ID	Gain	Amplification	Loss
9806	1, 12qA1.1qter	12qA1.1 , 12qF2	12qa1.1, 11qA1
7217	12		
4834	10qA4qter		2, 12, 18, 9qA5.3qter, 4qB3qter
4726	1		
4848	1, 12, 19		
4827		12qF2, 12qC1	
4836 ^{a,b}	1	12qA1.1 , 3qf3, 12qF1-2	3qa3, 17qe2, 17qe1.1
drb13 ^a	12	12qA1.1	

Amplicons at 12qA1.1 harboring *N-myc* gene are in bold.

^aSamples selected for ROMA analysis based on the presence of *N-myc* amplification detected by Southern blot.

^bTail DNA used for ROMA hybridization was not from the tumor-containing mouse; thus, polymorphisms could contribute to focal changes.

the *Rb/p130* DKO model, *N-myc* was found amplified in 3/16 samples, ranging from 6- to 17-fold (Figure 5B). *N-myc* amplifications may be more frequent in metastases in this model, as Southern blot analyses of 17 primary *Rb/p130* DKO tumors did not reveal amplification of the gene (data not shown). Of note, we did not have the matched primary tumors for those metastases that did exhibit *N-myc* amplification, and, therefore, we could not assess whether the amplification was specific to the metastases. Interestingly, from a series of 21 primary retinoblastomas from the *Rb/p107* DKO model, two tumors exhibited *N-myc* amplification (Figure 5C). A metastasis from one of these tumors (tumor 4459; Figure 5C) also exhibited amplification. *N-myc* amplification was not detected in seven other metastatic *Rb/p107* DKO tumors (data not shown). Taken together, we observed *N-myc* amplification in 2/28 *Rb/p107* DKO retinoblastomas.

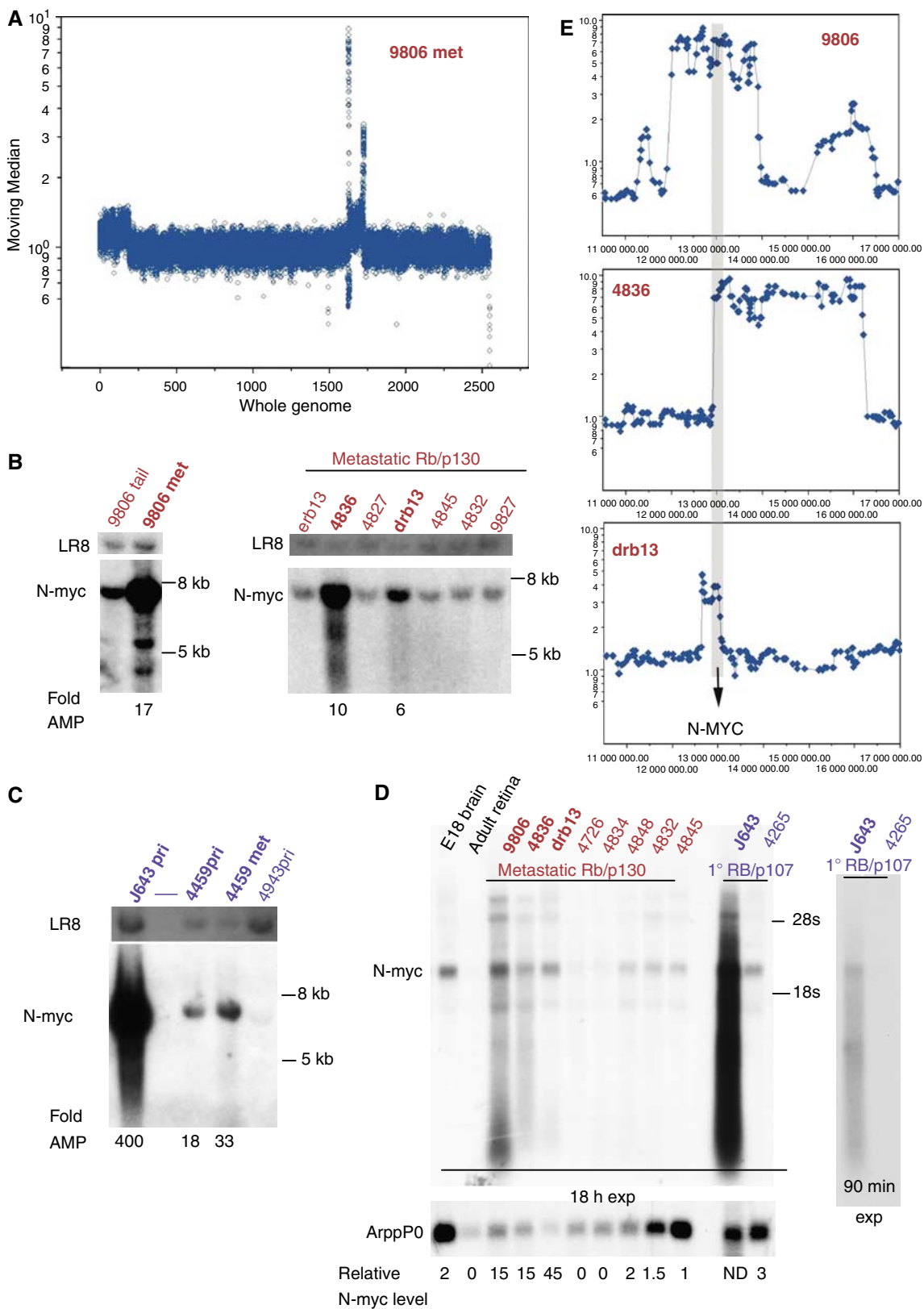
To determine whether *N-myc* was expressed in retinoblastomas with gene amplification, we performed Northern blot analyses. In metastatic *Rb/p130* DKO tumors, *N-myc* was found highly expressed in the samples that exhibited genomic amplification (Figure 5D). The primary tumor J643 from the *Rb/p107* DKO model, which exhibited a 400-fold gene amplification, expressed extremely high levels of *N-myc* transcript (Figure 5D). Quantitative RT-PCR confirmed that *N-myc* was overexpressed in tumors with genomic amplification, and demonstrated clearly detectable, but lower levels of *N-myc* in samples without amplification (Supplementary Figure 4). Interestingly, *C-myc* and *L-myc* were also found to be expressed in murine retinoblastomas (Supplementary Figure 5).

Although our initial observation of a 1.9 Mb amplicon in tumor 9806 implicated *N-myc* in selection for cells with DNA copy number increase in 12qA1.1, it remained a possibility that other co-amplified genes near *N-myc* were also selected for during tumor progression. To delineate the size of the *N-myc* amplicon and determine the minimal region amplified, we performed ROMA analyses on two additional samples positive for *N-myc* amplification by Southern blot. The *N-myc* amplicon from tumor Drb13 was 451 kb. Tumor 4836 exhibited a 3.3 Mb amplicon. Along with the 1.9 Mb amplicon from tumor 9806, the minimally overlapping region was only 136 kb in length (coordinates 12 937 244–13 073 187, UCSC

genome browser May 2004 build) (Figure 5E). Within this 136 kb region, *N-myc* is the only known gene present. This analysis strongly supports the candidacy of *N-myc* as the specific target of gene amplification in the murine retinoblastomas.

Discussion

Here, we describe novel mouse models of retinoblastoma that recapitulate important aspects of human retinoblastoma, both histologically and genetically. Our data address the



earliest stages of tumor development and implicate regionally restricted cells in tumor initiation. The fact that the tumors in these models can progress to the point of brain involvement and spread to local lymph nodes is also extremely important as such advanced tumors in humans are associated with very low survival (Jubran *et al*, 2004). Thus, these models may prove useful in testing therapies to improve the treatment of patients with advanced retinoblastoma. The amplification of the *N-myc* oncogene in a subset of tumors from the *Rb/p130* DKO and *Rb/p107* DKO mice provides further evidence that these models mirror genetic aspects of human retinoblastoma development.

The consistent and rapid tumorigenesis observed in the *Rb/p130* DKO model makes it particularly well suited for preclinical testing of anticancer agents and chemoprevention studies. Importantly, unlike several other models of retinoblastoma, this model does not rely on mutation or inactivation of *p53* (Windle *et al*, 1990; Howes *et al*, 1994; Zhang *et al*, 2004b; Dyer *et al*, 2005). In fact, *p53* loss is rarely observed in human retinoblastomas (Gallie *et al*, 1999) although there is recent evidence that an upstream regulator of *p53*, MDMX, is amplified in human retinoblastomas (Laurie *et al*, 2006). *p53* can be activated in human retinoblastoma cells (Laurie *et al*, 2006) and the *p53* pathway clearly influences treatment outcomes in many cancers (Soussi and Beroud, 2001). Thus, the maintenance of a potentially intact *p53* pathway in the *Rb/p130* DKO model may yield more accurate responses to therapy. Also, *p53* mutation might broaden the cell types that are capable of transformation following disruption of the pRB pathway function and thus complicate the identification of the cell of origin for human retinoblastoma.

Retinoblastoma origins

Retinoblastomas in the *Rb/p130* DKO model arose from a specific area in the extreme retina periphery with complete penetrance in *Rb/p130* DKO animals by 1 month of age. The regional specificity and high tumor frequency was particularly surprising owing to the degeneration of *Rb* and *p130* mutant cells away from this part of the retinal region (see Figure 2). These observations provide insights important for future identification of the tumor cell of origin. We observed extensive heterogeneity in expression of cell-type-specific markers in tumors. The heterogeneity in marker expression, including positive staining for syntaxin, calretinin and calbindin as well as some GFAP positivity, suggests that the cell of origin may be a multipotent cell capable of producing amacrine and horizontal cells and potentially

Müller cells. Our data are also consistent with a cell of origin that exhibits restricted potential. For example, some progenitor cells are biased toward horizontal and amacrine fates (Alexiades and Cepko, 1997). Interestingly, studies from fish and amphibians have implicated the ciliary marginal zone at the extreme periphery of retina as a location for adult stem cells (Reh and Fischer, 2001). In mice and humans, cells with stem cell properties have been isolated from the pigmented cell layer of the ciliary body, a peripheral structure adjacent to the neural retina (Tropepe *et al*, 2000). Future work will differentiate between stem, progenitor and transition cells as the target for transformation in this mouse model of retinoblastoma.

Localization of retinoblastomas to the extreme periphery of retina has not been described in other models of the disease. *Rb/p107* chimeras were reported to exhibit dysplastic retinas by E17.5, and tumors were proposed to arise from cells transformed at this time (Robanus-Maandag *et al*, 1998). We also previously observed severe disorganization throughout the retina at E18.5 in 100% of animals lacking *Rb* and *p107* (MacPherson *et al*, 2004). However, owing to the fact that *Rb/p107* DKO mice develop retinoblastomas at a lower frequency than *Rb/p130* DKO mice, we would suggest that this phenotype might be unlinked to tumor initiation. Chen *et al* (2004) noted that proliferation stopped by PND30 in *Rb/p107* DKO mice. In contrast, our BrdU-labeling studies indicate that although the vast majority of *Rb/p107* DKO cells exit the cell cycle by PND31, some cells concentrated at the extreme periphery of retina continue to proliferate (Supplementary Figure 3B and C). Our finding of lesions with histological characteristics of retinoblastoma specifically in this region in a subset of *Rb/p107* DKO animals at PND31 and PND60 implicates a peripheral cell of origin in the *Rb/p107* DKO model as well as in the *Rb/p130* DKO model.

We note that in humans, retinoblastomas can arise from cells in central or peripheral retina. Interestingly, a strong correlation between age at tumor detection and retinal topography has been reported in human bilateral retinoblastoma patients, with early retinoblastomas more frequently presenting in central retina and later retinoblastomas arising in the periphery of retina (Abramson and Gombos, 1996). Other studies have reported peripheral locations to new retinoblastomas that arise after treatment for initial retinoblastomas (Salmonsens *et al*, 1979; Shields *et al*, 2003). Thus, the murine models we describe may more resemble a subset of human retinoblastomas that arise from peripheral retina.

Figure 5 *N-Myc* amplification and overexpression in retinoblastomas. (A) ROMA moving median plot showing signal intensity plotted for the whole genome comparing tail (Cy3 labeled) and lymph node metastasis (Cy5 labeled) DNA from tumor 9806. Specific changes from this tumor detailed in Table I include gains of chromosomes 1 and 12, as well as two focal chromosome 12 amplicons. (B) Southern analysis of DNA from lymph node *Rb/p130* DKO retinoblastoma metastases or normal tail DNA. DNA was digested with *Eco*R1 and probed with an *N-myc* cDNA fragment. Following *N-myc* detection, blot was rehybridized to an *LR8* probe to control for loading. Fold amplification as assessed by phosphorimager analysis of the same blot is shown. Samples with amplification are highlighted in bold. (C) Southern analysis of *Rb/p107* DKO primary (pri) or metastatic (met) retinoblastomas. Hybridization with *LR8* probe was used as a loading control. Samples with amplification are highlighted in bold. (D) Northern analysis of *N-myc* expression in retinoblastomas. Samples with *N-myc* genomic amplification are highlighted in bold. *N-myc* levels were extremely high in *Rb/p107* DKO tumor J643. A lower exposure of the right side of this blot containing J643 is shown (right). Quantification of *N-myc* relative to ARPP P0 loading control shows highest expression in *N-myc*-amplified samples. (E) A core amplified region of 136 kb in murine retinoblastomas. The 12qA1.1 amplified regions of three murine retinoblastomas (9806, 4836 and drb13) are shown. Shaded area (136 kb in size; 12 937 244–13 073 187 UCSC May/2004 build) indicates the genomic area that is amplified in all three tumors. *N-myc* is the only RefSeq gene inside the core amplicon.

Rb/p107 versus Rb/p130 DKO retinoblastoma models

p107 and *p130* have overlapping functions, but significant differences also exist (Classon and Dyson, 2001). *p130* is more highly expressed in postmitotic cells and postnatal stages of retinal development whereas *p107* exhibits its highest expression in cycling cells and in embryonic stages of retinal development (Hurford *et al*, 1997; Spencer *et al*, 2005; Donovan *et al*, 2006). Consistent with these expression patterns, at E18 (a time of extensive proliferation in the retina), the combined loss of *Rb* and *p130* is phenotypically similar to loss of *Rb* alone. In contrast, the combined loss of *Rb* and *p107* at this stage led to a much more severe phenotype (MacPherson *et al*, 2004). Moreover, chimeras composed of cells mutant for *Rb* and *p130* or *Rb* and *p107* developed a range of novel tumors, but the tumor spectrum was different in the two settings (Dannenberg *et al*, 2004). In the present study, we directly compared the effects of the absence of *p130* and *p107* function on retinoblastoma development in the context of *Rb* mutation. We found that *p130* is a much stronger suppressor of retinoblastoma development than *p107*, with 100% of *Rb/p130* DKO animals developing tumors rapidly. The kinetics of tumor development suggests that loss of *Rb* and *p107* is not sufficient even for an early retinoblastoma to form. It is possible that *Rb/p107* DKO cells must abrogate a block to tumorigenesis caused by the presence of the remaining pocket protein family member, *p130*, in order to progress further.

Although the kinetics of tumorigenesis was different between *Rb/p130* and *Rb/p107* DKO models, the retinoblastomas that ultimately arose in these models were similar histologically and with respect to their site of origin. Tumors in both models also underwent metastatic progression to the brain and cervical lymph nodes. Strong similarities have also been reported for earlier models of retinoblastomas of these different genotypes (Robanus-Maandag *et al*, 1998; Chen *et al*, 2004; Dannenberg *et al*, 2004; MacPherson *et al*, 2004). Finally, the fact that both *Rb/p107* and *Rb/p130* DKO retinoblastomas exhibit *N-myc* gene amplification supports common mechanisms of cell transformation.

ROMA analysis

Based on the focal nature of tumor formation and the variability in the kinetics of tumor progression, we suspected that mutation of *Rb* family members was not sufficient for tumorigenesis. Therefore, to begin to characterize the tumors for additional genetic alterations, we used ROMA analysis (Lucito *et al*, 2003). We found that chromosome 12 and chromosome 1 were increased in copy number, each in four of eight of the total tumors examined (Table I). CGH analyses of human retinoblastoma have reported frequent chromosomal gains in 6p and 1q (Mairal *et al*, 2000; Chen *et al*, 2001; Lillington *et al*, 2003; Zielinski *et al*, 2005). The human 1q31–32 region undergoes chromosomal gain in over 50% of human retinoblastomas and is syntenic to murine chromosome 1. Possible candidate genes driving selection for 1q31–1q32 alterations, such as *KIF14A* (Corson *et al*, 2005) and *MDMX* (Laurie *et al*, 2006), also exhibit copy number gain in murine retinoblastomas, suggesting that some selective events in murine and human retinoblastomas may be identical. Larger studies comparing secondary alterations in human and murine retinoblastoma will help to identify the

genes that drive selection for chromosomal alterations in human retinoblastoma.

We focused our analysis of candidates from our ROMA data on the 12qA1.1 *N-myc*-containing amplicon. *N-myc* is highly amplified in neuroblastomas and amplification is associated with tumor progression (Brodeur *et al*, 1984). *N-myc* is also amplified in human retinoblastoma, along with many other genes on 2p. In our studies, high-resolution DNA copy number analysis pinpointed a common region of amplification consisting of just 136 kb. Within this region, *N-myc* is the only known gene present. *N-myc* has been implicated in many aspects of tumor biology and the specific reason for selection of cells with amplified *N-myc* in retinoblastoma progression is not known. Thus, the critical pathways downstream of *N-myc* in this system will be important to elucidate. *N-myc* amplification is likely not critical for the earliest steps in tumorigenesis in our *Rb/p130* DKOs as 100% of animals exhibit bilateral lesions early. We observed these amplifications in metastatic tumors lacking *Rb* and *p130* as well as in primary tumors lacking *Rb* and *p107*. It is possible that the loss of *Rb* and *p107* is not sufficient even for early tumors, and *N-myc* amplification may help these cells overcome a proliferative block. Alternatively, *N-myc* may have a primary role later in tumor progression. Although *N-myc* amplification occurs only in a subset of retinoblastomas, it is possible that pathways downstream of *N-myc* may be activated following other secondary alterations that occur in retinoblastomas. Also, small changes in *N-myc* dosage through low-level chromosome 12 gain may confer a selective advantage upon tumor cells. A large-scale analysis of early and late lesions in both *Rb/p107* and *Rb/p130* DKO models will help to determine the nature and order of changes that occur as retinoblastoma progresses in the mouse. These data will undoubtedly aid in the understanding of the molecular genetic events that contribute to retinoblastoma development in humans.

Materials and methods

Mice

All mouse protocols were approved by animal care committees at the Massachusetts Institute of Technology and the Carnegie Institution. The generation of *p107*^{-/-} (Lee *et al*, 1996) and *Rb*^{lox/lox} (Sage *et al*, 2003) animals has been described. *Pax6* α -enhancer *Cre* mice (Marquardt *et al*, 2001) were bred with *Rb*^{lox/lox}; *p130*^{-/-} or *Rb*^{lox/lox}; *p107*^{-/-} animals. The *p130* mutant allele used in this study is a new allele with a deletion of *p130* exon 2 obtained after Cre-mediated recombination of a conditional allele where *p130* exon 2 is flanked by *loxP* sites (Tyler Jacks and Julien Sage, manuscript in preparation). We used this new allele instead of the previously described *p130* null allele (Cobrinik *et al*, 1996) because this deletion of exon 2 minimizes the chances of alternative splicing events that may produce truncated forms of p130. Mice were maintained on a mixed C57Bl6; 129SvJ; FvB/N background. For full necropsy analysis, inner organs were fixed in 3.7% formaldehyde in PBS, whereas bones and the skull were fixed in Bouin's fixative before processing through an ethanol series and xylene to paraffin. Methods for indirect ophthalmoscopy and fundus photography are provided in Supplementary Data.

Immunohistochemistry and beta-galactosidase histochemistry

Eyes were fixed in Bouin's fixative or 3.7% formaldehyde in PBS overnight before being processed through to paraffin. Retina analysis was performed on 4 μ m thick paraffin-embedded sections and immunostaining was performed on horizontal sections at the level of the optic nerve head. Immunohistochemistry and BrdU

analysis were performed essentially as described (MacPherson *et al*, 2003). The following antibodies were used: syntaxin (Sigma), calretinin (SWANT), calbindin (Chemicon), M-opsin (C Craft and X Xhu, UCLA), PKC- α (PharMingen), GLAST (Abcam), active caspase3 (Cell Signaling), Tuj1 (Covance). Beta-galactosidase histochemistry was performed as described (MacPherson *et al*, 2004).

Quantitative PCR and Southern and Northern analyses

Methods for real-time RT-PCR and Northern and Southern blot analyses are included in Supplementary Data.

ROMA

Genomic DNA from murine retinoblastomas and matching tails was prepared using the conventional protease-K method, followed by extensive phenol and phenol/chloroform extraction. BglII-derived genome representations were labeled with Cy5 (tumor) and Cy3 (tail/matched normal) by random - priming. The hybridizations to 84k oligonucleotide-based ROMA arrays (Nimblegen Systems, Reykjavic, Iceland) were carried out essentially as described (Lucito *et al*, 2003). The oligonucleotide sequence design of the murine ROMA arrays is described elsewhere (Lakshmi *et al*, 2006). All array images were acquired with an Axon GenePix 4000B scanner. The raw array data were globally normalized and a moving window of

five data points was used to smoothen the raw data by assigning the median value of the moving window to each central data point.

Supplementary data

Supplementary data are available at *The EMBO Journal* Online (<http://www.embojournal.org>).

Acknowledgements

We thank D Crowley and M Brown for histology preparation and K Nguyen for performing ROMA experiments. We also thank P Gruss, R Ashery Padan and T Marquardt for the *Pax6* α -enhancer-Cre mice, P Soriano for the *R26R* mice, as well as C Craft and X Zhu for antibodies to M-opsin. *LR8* probe was a gift of C Bassing and *ARPP P0* probe a gift of E Flores. We thank CM Fan, M McLaughlin and J Sage for critical reading of the manuscript. This work was supported by grant PO1-CA42063 from the National Cancer Institute and, partially, by Cancer Center Support (core) grant P30-CA14051 from the National Cancer Institute. DM is supported by a grant from Joan's Legacy Foundation. SM was supported by Gifts to the Retina Genetics Fund and Mukai Fund, Massachusetts Eye and Ear Infirmary. TJ is a Howard Hughes Investigator.

References

- Abramson DH, Gombos DS (1996) The topography of bilateral retinoblastoma lesions. *Retina* **16**: 232–239
- Alexiades MR, Cepko CL (1997) Subsets of retinal progenitors display temporally regulated and distinct biases in the fates of their progeny. *Development* **124**: 1119–1131
- Breuder GM, Seeger RC, Schwab M, Varmus HE, Bishop JM (1984) Amplification of N-myc in untreated human neuroblastomas correlates with advanced disease stage. *Science* **224**: 1121–1124
- Chen D, Gallie BL, Squire JA (2001) Minimal regions of chromosomal imbalance in retinoblastoma detected by comparative genomic hybridization. *Cancer Genet Cytogenet* **129**: 57–63
- Chen D, Livne-bar I, Vanderluit JL, Slack RS, Agochiya M, Bremner R (2004) Cell-specific effects of RB or RB/p107 loss on retinal development implicate an intrinsically death-resistant cell-of-origin in retinoblastoma. *Cancer Cell* **5**: 539–551
- Clarke AR, Maandag ER, van Roon M, van der Lugt NM, van der Valk M, Hooper ML, Berns A, te Riele H (1992) Requirement for a functional Rb-1 gene in murine development. *Nature* **359**: 328–330
- Classon M, Dyson N (2001) p107 and p130: versatile proteins with interesting pockets. *Exp Cell Res* **264**: 135–147
- Cobrinik D, Lee MH, Hannon G, Mulligan G, Bronson RT, Dyson N, Harlow E, Beach D, Weinberg RA, Jacks T (1996) Shared role of the pRB-related p130 and p107 proteins in limb development. *Genes Dev* **10**: 1633–1644
- Corson TW, Huang A, Tsao MS, Gallie BL (2005) KIF14 is a candidate oncogene in the 1q minimal region of genomic gain in multiple cancers. *Oncogene* **24**: 4741–4753
- Dannenberg JH, Schuijff L, Dekker M, van der Valk M, te Riele H (2004) Tissue-specific tumor suppressor activity of retinoblastoma gene homologs p107 and p130. *Genes Dev* **18**: 2952–2962
- Donovan S, Schweers B, Martins R, Johnson D, Dyer MA (2006) Compensation by tumor suppressor genes during retinal development in mice and humans. *BMC Biol* **4**: 14
- Dyer MA, Rodriguez-Galindo C, Wilson MW (2005) Use of pre-clinical models to improve treatment of retinoblastoma. *PLoS Med* **2**: e332
- Gallie BL, Campbell C, Devlin H, Duckett A, Squire JA (1999) Developmental basis of retinal-specific induction of cancer by RB mutation. *Cancer Res* **59**: 1731s–1735s
- Haigis K, Sage J, Glickman J, Shafer S, Jacks T (2006) The related retinoblastoma (pRb) and p130 proteins cooperate to regulate homeostasis in the intestinal epithelium. *J Biol Chem* **281**: 638–647
- Howes KA, Ransom N, Papermaster DS, Lasudry JG, Albert DM, Windle JJ (1994) Apoptosis or retinoblastoma: alternative fates of photoreceptors expressing the HPV-16 E7 gene in the presence or absence of p53. *Genes Dev* **8**: 1300–1310
- Hurford Jr RK, Cobrinik D, Lee MH, Dyson N (1997) pRB and p107/p130 are required for the regulated expression of different sets of E2F responsive genes. *Genes Dev* **11**: 1447–1463
- Jacks T, Fazeli A, Schmitt EM, Bronson RT, Goodell MA, Weinberg RA (1992) Effects of an Rb mutation in the mouse. *Nature* **359**: 295–300
- Jubran RF, Erdreich-Epstein A, Butturini A, Murphree AL, Villablanca JG (2004) Approaches to treatment for extraocular retinoblastoma: Children's Hospital Los Angeles experience. *J Pediatr Hematol Oncol* **26**: 31–34
- Knudson Jr AG (1971) Mutation and cancer: statistical study of retinoblastoma. *Proc Natl Acad Sci USA* **68**: 820–823
- Lakshmi B, Hall IM, Egan C, Alexander J, Leotta A, Healy J, Zender L, Spector MS, Xue W, Lowe SW, Wigler M, Lucito R (2006) Mouse genomic representational oligonucleotide microarray analysis: detection of copy number variations in normal and tumor specimens. *Proc Natl Acad Sci USA* **103**: 11234–11239
- Laurie NA, Donovan SL, Shih CS, Zhang J, Mills N, Fuller C, Teunisse A, Lam S, Ramos Y, Mohan A, Johnson D, Wilson M, Rodriguez-Galindo C, Quarto M, Francoz S, Mendrysa SM, Guy RK, Marine JC, Jochemsen AG, Dyer MA (2006) Inactivation of the p53 pathway in retinoblastoma. *Nature* **444**: 61–66
- Lee EY, Chang CY, Hu N, Wang YC, Lai CC, Herrup K, Lee WH, Bradley A (1992) Mice deficient for Rb are nonviable and show defects in neurogenesis and haematopoiesis. *Nature* **359**: 288–294
- Lee MH, Williams BO, Mulligan G, Mukai S, Bronson RT, Dyson N, Harlow E, Jacks T (1996) Targeted disruption of p107: functional overlap between p107 and Rb. *Genes Dev* **10**: 1621–1632
- Lee WH, Murphree AL, Benedict WF (1984) Expression and amplification of the N-myc gene in primary retinoblastoma. *Nature* **309**: 458–460
- Lillington DM, Goff LK, Kingston JE, Onadim Z, Price E, Domizio P, Young BD (2002) High level amplification of N-MYC is not associated with adverse histology or outcome in primary retinoblastoma tumours. *Br J Cancer* **87**: 779–782
- Lillington DM, Kingston JE, Coen PG, Price E, Hungerford J, Domizio P, Young BD, Onadim Z (2003) Comparative genomic hybridization of 49 primary retinoblastoma tumors identifies chromosomal regions associated with histopathology, progression, and patient outcome. *Genes Chromosomes Cancer* **36**: 121–128
- Lucito R, Healy J, Alexander J, Reiner A, Esposito D, Chi M, Rodgers L, Brady A, Sebat J, Troge J, West JA, Rostan S, Nguyen KC, Powers S, Ye KQ, Olshen A, Venkatraman E, Norton L, Wigler M (2003) Representational oligonucleotide microarray analysis: a high-resolution method to detect genome copy number variation. *Genome Res* **13**: 2291–2305

- Maandag EC, van der Valk M, Vlaar M, Feltkamp C, O'Brien J, van Roon M, van der Lugt N, Berns A, te Riele H (1994) Developmental rescue of an embryonic-lethal mutation in the retinoblastoma gene in chimeric mice. *EMBO J* **13**: 4260–4268
- MacPherson D, Sage J, Crowley D, Trumpp A, Bronson RT, Jacks T (2003) Conditional mutation of Rb causes cell cycle defects without apoptosis in the central nervous system. *Mol Cell Biol* **23**: 1044–1053
- MacPherson D, Sage J, Kim T, Ho D, McLaughlin ME, Jacks T (2004) Cell type-specific effects of Rb deletion in the murine retina. *Genes Dev* **18**: 1681–1694
- Mairal A, Pinglier E, Gilbert E, Peter M, Validire P, Desjardins L, Doz F, Aurias A, Couturier J (2000) Detection of chromosome imbalances in retinoblastoma by parallel karyotype and CGH analyses. *Genes Chromosomes Cancer* **28**: 370–379
- Marquardt T, Ashery-Padan R, Andrejewski N, Scardigli R, Guillemot F, Gruss P (2001) Pax6 is required for the multipotent state of retinal progenitor cells. *Cell* **105**: 43–55
- Pinkel D, Albertson DG (2005) Array comparative genomic hybridization and its applications in cancer. *Nat Genet* **37**: S11–S17
- Reh TA, Fischer AJ (2001) Stem cells in the vertebrate retina. *Brain Behav Evol* **58**: 296–305
- Robanus-Maandag E, Dekker M, van der Valk M, Carrozza ML, Jeanny JC, Dannenberg JH, Berns A, te Riele H (1998) p107 is a suppressor of retinoblastoma development in pRb-deficient mice. *Genes Dev* **12**: 1599–1609
- Sage J, Miller AL, Perez-Mancera PA, Wysocki JM, Jacks T (2003) Acute mutation of retinoblastoma gene function is sufficient for cell cycle re-entry. *Nature* **424**: 223–228
- Salmonsens PC, Ellsworth RM, Kitchin FD (1979) The occurrence of new retinoblastomas after treatment. *Ophthalmology* **86**: 837–843
- Sherr CJ (1996) Cancer cell cycles. *Science* **274**: 1672–1677
- Shields CL, Shelil A, Cater J, Meadows AT, Shields JA (2003) Development of new retinoblastomas after 6 cycles of chemoreduction for retinoblastoma in 162 eyes of 106 consecutive patients. *Arch Ophthalmol* **121**: 1571–1576
- Shields CL, Shields JA, Baez K, Cater JR, De Potter P (1994) Optic nerve invasion of retinoblastoma. Metastatic potential and clinical risk factors. *Cancer* **73**: 692–698
- Soussi T, Beroud C (2001) Assessing TP53 status in human tumours to evaluate clinical outcome. *Nat Rev Cancer* **1**: 233–240
- Spencer C, Pajovic S, Devlin H, Dinh QD, Corson TW, Gallie BL (2005) Distinct patterns of expression of the RB gene family in mouse and human retina. *Gene Expr Patterns* **5**: 687–694
- Squire J, Goddard AD, Canton M, Becker A, Phillips RA, Gallie BL (1986) Tumour induction by the retinoblastoma mutation is independent of N-myc expression. *Nature* **322**: 555–557
- Tropepe V, Coles BL, Chiasson BJ, Horsford DJ, Elia AJ, McInnes RR, van der Kooy D (2000) Retinal stem cells in the adult mammalian eye. *Science* **287**: 2032–2036
- Williams BO, Schmitt EM, Remington L, Bronson RT, Albert DM, Weinberg RA, Jacks T (1994) Extensive contribution of Rb-deficient cells to adult chimeric mice with limited histopathological consequences. *EMBO J* **13**: 4251–4259
- Windle JJ, Albert DM, O'Brien JM, Marcus DM, Distèche CM, Bernards R, Mellon PL (1990) Retinoblastoma in transgenic mice. *Nature* **343**: 665–669
- Wu L, de Bruin A, Saavedra HI, Starovic M, Trimboli A, Yang Y, Opavska J, Wilson P, Thompson JC, Ostrowski MC, Rosol TJ, Woollett LA, Weinstein M, Cross JC, Robinson ML, Leone G (2003) Extra-embryonic function of Rb is essential for embryonic development and viability. *Nature* **421**: 942–947
- Yuge K, Nakajima M, Uemura Y, Miki H, Uyama M, Tsubura A (1995) Immunohistochemical features of the human retina and retinoblastoma. *Virchows Arch* **426**: 571–575
- Zhang J, Gray J, Wu L, Leone G, Rowan S, Cepko CL, Zhu X, Craft CM, Dyer MA (2004a) Rb regulates proliferation and rod photoreceptor development in the mouse retina. *Nat Genet* **36**: 351–360
- Zhang J, Schweers B, Dyer MA (2004b) The first knockout mouse model of retinoblastoma. *Cell Cycle* **3**: 952–959
- Zhu X, Brown B, Li A, Mears AJ, Swaroop A, Craft CM (2003) GRK1-dependent phosphorylation of S and M opsins and their binding to cone arrestin during cone phototransduction in the mouse retina. *J Neurosci* **23**: 6152–6160
- Zielinski B, Gratiás S, Toedt G, Mendrzyk F, Stange DE, Radlwimmer B, Lohmann DR, Lichter P (2005) Detection of chromosomal imbalances in retinoblastoma by matrix-based comparative genomic hybridization. *Genes Chromosomes Cancer* **43**: 294–301